Wide-Band Prediction of Stirrer Efficiency in Over-the-Air Test with Variable Loading Conditions

Andréa Cozza

Wide-Band Prediction of Stirrer Efficiency in Over-the-Air Test with Variable Loading Conditions

Andrea Cozza, *Senior Member, IEEE*

***Abstract*—This letter introduces a fast procedure for predicting the performance of mechanical stirrers used in reverberation chambers (RCs) for over-the-air (OTA) tests of wireless communication devices, measured by the auto-correlation function (ACF) between stirrer-generated samples. The procedure is tested for three different stirrers in an RC where eleven load cases create widely different power-delay profiles, with a time spread spanning more than two orders of magnitude. The proposed procedure is shown to accurately predict the ACF and, therefore, how the number of independent samples is affected for each of the eleven RC load cases over an 8 GHz band, by only using data measured in unloaded conditions at 12 frequencies up to 4 GHz. Adding a second dataset with the RC loaded further reduces the uncertainty of the predictions, which are found to be more accurate than direct measurements, thanks to the regularizing effect of a wide-band parametric stirrer efficiency model. This method significantly reduces preliminary test time, providing a quantitative tool to evaluate beforehand the limitations of a stirrer's performance in OTA tests.**

***Index Terms*—Reverberation chamber, mechanical stirrer, stirring efficiency, auto-correlation function, over-the-air test, power-delay profile, loading.**

I. Introduction

OVER the last two decades reverberation chambers (RCs) have taken a leading role in the evaluation of the performance of wireless communication devices in over-the-air (OTA) tests. Their ability to create complex multi-path environments set them apart from traditional anechoic facilities [1]–[4], especially with the ever-increasing reliance on multi-antenna systems. The presence of devices such as mechanical stirrers and turntables enable the generation of large sets of random channel realizations, ensuring the accurate statistical analysis of results from OTA tests.

OTA tests require the control of several features of the propagation channels emulated in an RC, such as the spread time τ_a associated with the power-delay profile, anisotropy in the directions of arrival, K factor for Rician channels, coherence bandwidth, etc. These are often, at least in part, controlled by precisely loading the RC with lossy foam absorbers [2], [5]–[7]. This approach, while effective, has been shown to increase the auto-correlation function (ACF) $\hat{R}$ estimated from measured samples, implying a reduced number N_e of independent samples that a mechanical stirrer can generate. This, in turn, increases the uncertainty budget of OTA tests [8]–[12], which require a minimum threshold for N_e, as also called for by standardization organizations such as CTIA and 3GPP [13], [14]. In current practice, N_e is estimated experimentally, often based on sample ACF, which requires repeated time-consuming preliminary tests whenever the RC loading is modified [7], [11], [15].

As opposed to this practice, it has recently been proven that the ACF between stirrer-generated samples can in fact be predicted, by first estimating the intrinsic stirrer efficiency parameters (ISEP): $R_s(\nu)$, modelling the direction-averaged correlation in the stirrer forward scattering, as a function of the frequency ν; $\tau_o(\nu) = \tau_s(\nu)/V$, with V the RC volume and τ_s the stirring coherence time, i.e., the time constant of the loss of coherence in the time-domain (TD) response of the RC, when the stirrer position is modified by an angle $k\Delta\psi$. The k-lag ACF $R(\nu;k)$ of stirrer-generated samples was shown in [16], [17] to be simply explained by the stirrer ISEP and the RC power-decay time (or spread time) $\tau_a(\nu)$, by

$$R(\nu;k) = \frac{R_s(\nu;k)}{1+\tau_a(\nu)/\tau_s(\nu;k)}. \tag{1}$$

Knowledge of a stirrer's ISEP thus provides a simple means of predicting how a stirrer efficiency evolves as the RC loading is modified [16], but estimating them precisely and efficiently is not trivial. Eq. (1) suggests that R_s and τ_s could be estimated from the sample-evaluated ACF $\hat{R}$. In practice, the confidence interval of $\hat{R}$ is far from negligible [9], [18], increasing the risk of imprecise ISEP estimates.

The approach applied in [16] was instead based on the analysis of the TD ACF computed over a narrow bandwidth B_T, but is marred by multiple limitations: 1) for a highly efficient stirring, τ_s could become smaller than the time resolution $1/B_T$, making it difficult to estimate the ISEP over a short time window; 2) for poor stirring, τ_s could instead become larger than the maximum time-window $1/\Delta f$ afforded by a frequency step Δf, leading to time aliasing and thus an inaccurate estimate; 3) a TD formulation is complicated by the need to identify the time of the beginning of the ACF, which is not known beforehand, since it depends on the joint cavity and stirrer response.

This letter introduces an alternative approach to estimate the ISEP, based on frequency-domain (FD) results, avoiding the shortcomings of the TD approach. It also avoids the need for the large frequency sample collections required by TD analyses of RC responses, while using the FD ACF, which is a more common metric for RC users. This new method is detailed in Sec. II and tested in an RC with variable loading conditions described in Sec. III. Results reported in Sec. IV confirm the accuracy of the proposed procedure and its ability to predict a stirrer performance by only requiring a very

A. Cozza is with the Group of Electrical Engineering - Paris (GeePs), CNRS UMR 8507, CentraleSupélec, Université Paris-Saclay, Sorbonne Université, 11 rue Joliot-Curie, Plateau de Moulon 91192 Gif-sur-Yvette CEDEX, France (email: andrea.cozza@ieee.org).

limited number of data, mostly relying on tests carried out in an unloaded RC.

II. Frequency-domain ISEP identification

The limitations of estimating the ISEP in TD can be overcome by enforcing a continuity in their frequency evolution, which acts as a regularizing mechanism. Extensive experiments reported in [17] confirmed that for a stirrer with a surface area A_s, $\tau_s \sim \lambda^2/A_s$ with λ the wavelength, suggesting that surface scattering is the main physical mechanism, as first observed in [19]. R_s was also found to evolve smoothly over frequency, although no straightforward connection was established with the stirrer features. Shared features were $R_s \to 1$ as the frequency decreased, with a frequency response closely approaching a second-order polynomial.

Based on these observations, we introduce the following parametric ISEP models

$$R_s(\nu; b_1, b_2) = 1/\left(1 + (\nu/b_1)^{b_2}\right) \ , \ \tau_s(\nu; b_3) = b_3/\nu^2, \quad (2)$$

defined by three parameters $\boldsymbol{b} = [b_1, b_2, b_3]$. The inverted S-shape function for R_s is controlled by b_1, representing the frequency at which $R_s(b_1) = 0.5$, with b_2 setting the steepness of R_s; b_3 is expected to be inversely proportional to the stirrer surface A_s. The parameters $\boldsymbol{b}$ can be estimated from a least-square regression, fitting (1) to experimental results of the ACF $\hat{R}(\nu)$, as discussed later in this section. For the unloaded RC the ACF will be noted as $\hat{R}_1$, and its power-decay time $\tau_{a,1}$.

It is useful to define the cutoff frequency f_o at which $\tau_{a,1} = \tau_s$, found for $f_o^2 = b_3/\tau_{a,1}$. For $\nu < f_o$, (1) would be mostly dominated by R_s, while for $\nu > f_o$ it would be dominated by $R_s\tau_s$. Enforcing the physical response $1/\nu^2$ on τ_s with (2) allows to effectively, though not completely, unmix the contributions of R_s and τ_s. For this approach to succeed, the ACF $\hat{R}$ should be evaluated at least up to f_o.

The overall accuracy is significantly improved when another ACF, $\hat{R}_2$, is also available for a loaded case, with a power-decay time $\tau_{a,2} \ll \tau_{a,1}$. This condition ensures that $\hat{R}_2$ now features R_s more prominently, making it more readily accessible, improving at the same time the estimate of τ_s.

The ISEP model parameters $\boldsymbol{b}$ are then found by means of a non-linear least-square (NLLS) regression, fitting (1), and therefore the ISEP models (2), to the experimentally evaluated N_F frequency samples of the ACF, for the N_L available load cases, according to the cost function

$$J(\boldsymbol{b}) = \sum_{l=1}^{N_L} \sum_{k=1}^{N_F} w_{kl} \left| R(\nu_k; \tau_{a,l}, \boldsymbol{b}) - \hat{R}_l(\nu_k; \tau_{a,l}) \right|^2 \quad (3)$$

with $\hat{R}_l(\nu_k; \tau_{a,l})$ the ACF computed at the frequency ν_k from measurements obtained in the l-th case. Weights w_{kl} must be applied in the regression, since the ACF samples are heteroscedastic, i.e., they do not share the same variance [20]. Indeed, for an ACF equal to r, the sample variance for N_s samples is $\sigma^2 = (1 - r^2)^2/(N_s - 2)$ [21]. Weights are therefore set to $w_{kl} = \sigma_l^{-2}(\nu_k)$, giving less leverage to low-correlation samples, since less accurate. The cost function $J(\boldsymbol{b})$ is minimized applying Nelder-Mead search algorithm [22], with the double advantage of avoiding the computation of derivatives, and a more robust handling of local minima.

As with any optimization algorithm, the choice of initial values for $\boldsymbol{b}$ is critical. In order to improve the robustness of the proposed procedure, a simpler parabolic model is used first for estimating R_s from the unloaded RC data,

$$R_s(\nu; b_o) = (b_o - \nu)^2/b_o^2 \quad (4)$$

based on a single parameter, thus converging more reliably. Since $R_s(b_1) = 0.5$, b_o directly provides an estimate for b_1, as $b_1 = b_o(1 - 1/\sqrt{2}) \simeq 0.29 b_o$.

The proposed procedure covers the steps described below, with initial values for the model parameters given in brackets and NLLS results in parenthesis. The parameters resulting from the unloaded tests are marked as primed quantities, those including the loaded tests are double primed.

Phase 1 Unloaded RC

1: **set** $f_{\max}$
2: **estimate** $\tau_{a,1}(\nu)$ and the ACF $\hat{R}_1(\nu; \tau_{a,1})$
3: **minimize** $J(b_o, b_3)$ for $N_L = 1$ with R_s model (4) $[10 f_{max}, 0] \to (b_o, b_3')$
4: $f_o \leftarrow \sqrt{b_3'/\tau_{a,1}}$
5: **if** $f_o > f_{\max}$ **then set** $f_{\max} > f_o$, **go to** 1
6: $b_1' \leftarrow 0.29 b_o$

Phase 2 Loaded RC

7: **load** the RC s.t. $\tau_{a,2} < \tau_{a,1}/10$ and **estimate** $\hat{R}_2(\nu; \tau_{a,2})$
8: **minimize** $J(b_1, b_2, b_3)$ for $N_L = 2$ with R_s model (2) $[b_1', 1, b_3'] \to (b_1'', b_2'', b_3'')$

Once the ISEP are identified, the ACF can be predicted by means of (1), according to the τ_a required for the OTA test. The effective number of independent samples can then be estimated as discussed in [23].

III. Experiments

The proposed procedure was tested in an aluminium-alloy reverberation chamber, with dimensions $0.75 \times 1 \times 2.2$ m^3, for a volume $V = 1.65$ m^3, shown in Fig. 1(a). The RC has a mechanical stirrer mounted on its ceiling, with six removable dihedral elements, built from 15×30 cm^2 copper plates.

Two monocone antennas were used, one 40 cm above the floor and the other over the left wall. The S_{21} between the antennas was measured for each stirrer step over 50 frequency samples uniformly distributed from 0.5 to 8 GHz, using a vector network analyzer from Rohde & Schwarz, model ZVB8. Alternatively, S_{11} measurements from a single antenna may also be used. The stirrer was rotated over a full turn over 200 steps per test case, i.e. for $\Delta\psi = 1.8°$, recording the S_{21} at each step.

The RC was progressively loaded introducing foam absorbers, repeating the above measurement process each time. Absorbers were distributed over the RC walls and floor, as well as over its door, as shown in Fig. 1(b), using double-sided tape. In all, eleven load cases were tested, as detailed in Fig. 2, creating a very wide range of power-decay time

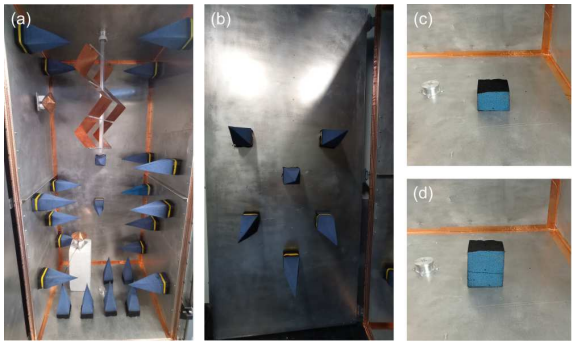

Fig. 1: Experimental setup with foam absorbers distributed in the RC (a) and on its door (b). The two small loads used for cases 2 and 3 (cf. Fig. 2) are shown in (c) and (d).

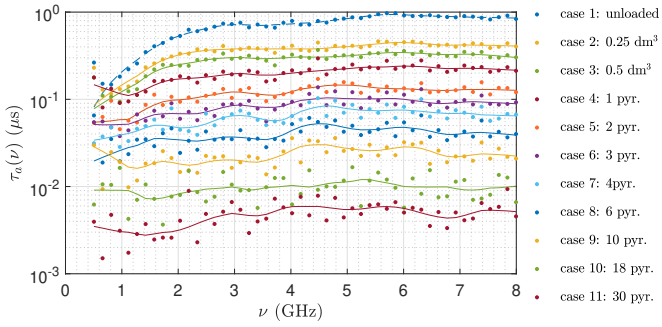

Fig. 2: Power-decay time τ_a for the eleven load cases, and the number of foam pyramids involved. Solid lines are the result of lowess smoothing.

scenarios, as required in OTA tests [3], [4], [24], [25]. These results are fundamental in order to assess the ability of the proposed procedure to predict how the ACF is modified by the RC loading. The power-decay time was estimated using the FD approach, based on the RC Q factor, as $\tau_a = Q/2\pi\nu$ [24], which requires compensating the low-frequency antenna mismatch, instead of the TD one [26], since the former requires far less frequency samples, thus speeding up the tests.

Fig. 2 shows that τ_a spans more than two orders of magnitude, from 1 μs for case 1, down to about 5 ns for case11, thus moving from a very highly reverberant medium to conditions close to free space. This process was repeated for each of the three stirrers, with 2, 4 and 6 dihedral elements. Since power loss in an RC is quickly dominated by dissipation in foam absorbers, $\tau_a(\nu)$ is expected to be flat, with $\tau_a \simeq V/2\pi c S_{abs}$ [27], where c is the speed of light and S_{abs} the absorption cross section.

IV. Results

The sample ACF $\hat{R}$ was computed for each load case for the three stirrers, for a sample lag $k \in [1, 3]$, corresponding to different choices of stirring step. Since the stirring efficiency increases with a larger step, τ_s also decreases, which in turn is equivalent to dealing with a larger stirrer. Studying the results for a larger k thus also extends the range of validity of the procedure described in Sec. II and provides insight into how RC loading affects more efficient stirring mechanisms.

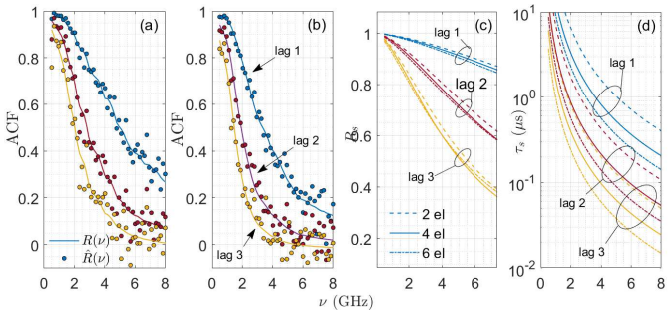

Fig. 3: Parametric ISEP model: ACF data fit for unloaded case for the (a) two- and (b) six-element stirrer respectively, smoothed across three samples for an easier comparison; (c-d) reference ISEP estimated using the eleven load-case datasets.

TABLE I: Reference ISEP-model results

# el.	k	f_o (GHz)	ΔR rms	ΔR 95%	$b_1^\star$ (GHz)	$b_2^\star$ -	$b_3^\star$ (THz)	a_o (μs)	b_1' (GHz)	b_3' (THz)
2	1	5.3	0.01	0.03	22.4	1.61	27.2	16.5	42.8	25.1
	2	3.0	0.02	0.05	9.63	1.59	7.14	4.32	11.7	7.37
	3	2.2	0.03	0.06	5.55	1.61	3.26	1.97	5.00	4.06
4	1	4.0	0.02	0.03	22.1	1.53	13.9	16.8	18.9	16.1
	2	2.2	0.02	0.05	9.02	1.54	3.55	4.30	10.4	3.44
	3	1.9	0.03	0.07	5.14	1.57	1.60	1.93	9.19	1.34
6	1	3.8	0.02	0.04	24.6	1.36	9.64	17.5	17.6	10.7
	2	2.0	0.03	0.06	9.27	1.41	2.32	4.22	6.43	2.83
	3	1.6	0.04	0.08	5.31	1.45	0.95	1.73	3.17	1.48

Data for the unloaded RC (case 1) were first used to estimate the stirrers ISEP. The steps in Phase 1 yield a regression $R(\nu)$ closely fitting the ACF shown in Figs. 3(a-b), confirming that the ACF can be explained over a wide band using just the two scalar parameters b_o and b_3, together with τ_a.

In order to validate the accuracy of the procedure in Sec. II, we need reference values for the ISEP. The datasets collected for the eleven load cases (Sec. III) share the same ISEP, but because of their increasing loading present different values of τ_a and thus of the ACF. Including all these datasets in Phase 2, with $N_L = 11$, yields the best estimate of the ISEP.

The results of this regression are presented in Figs. 3(c-d), showing that all stirrer models share a similar R_s, which decreases with higher lags; it is also confirmed that τ_s is inversely proportional to the stirrer surface A_s, for any choice of k. This property implies that $b_3 = a_o V c^2/A_s$, where the same a_o should thus be found for the three stirrers.

Tab. I presents the ISEP-model parameters $\boldsymbol{b}$ obtained for these reference results, marked by a star. The root-mean-square (rms) of the ACF residual error $\Delta R{=}R - \hat{R}$ across the 11 load cases is mostly smaller than 0.04, with a 95 % confidence interval (CI) at worst reaching 0.08. These results confirm that (2) can efficiently represent the stirrer performance over a wide band for a very large range of RC loading conditions. As expected, the area-independent a_o differs by only about 10 % across the three stirrers, for any stirrer step.

Tab. I also shows that b_3' obtained with (4) from the unloaded case accurately estimates the reference $b_3^\star$, i.e., it provides a good initial value for Phase 2. Instead, the estimate

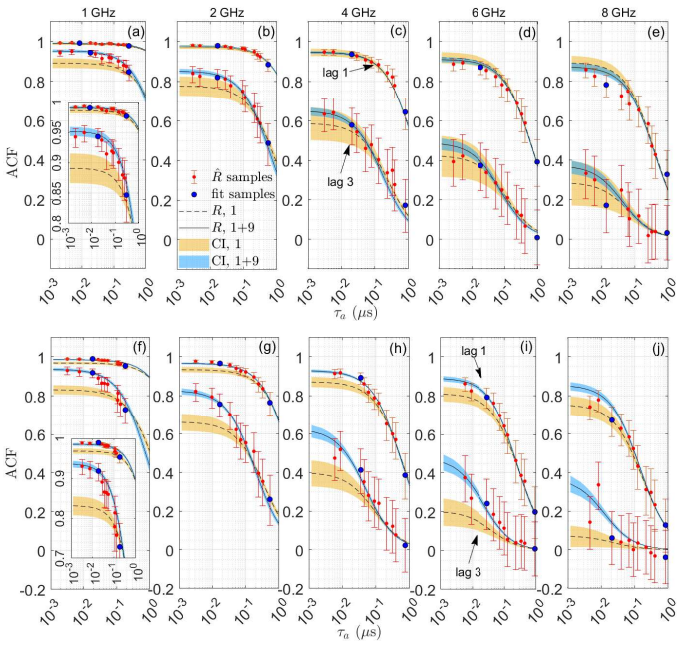

Fig. 4: ACF vs. loading for the two- and six-el. stirrers (top and bottom rows), for k={1, 3}. Blue discs mark the data used by the ISEP identification. Error bars show the 95% CI of $\hat{R}$.

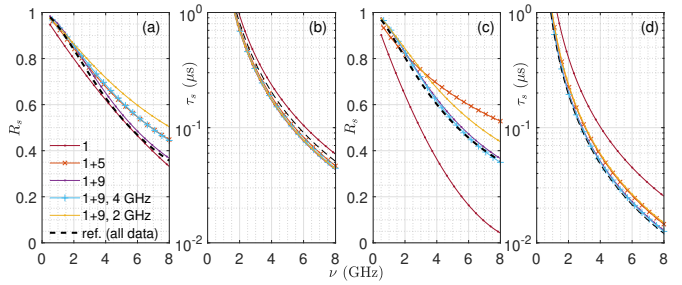

Fig. 5: ISEP for the two- (a-b) and six-element (c-d) stirrers, k=3, estimated for different choices of load cases and $f_{\max}$.

b_1' is less precise in two cases with $k = 3$. Having access to b_3 directly yields the cutoff frequency f_o, with Tab. I showing that it only exceeds 4 GHz for one case, hence the ISEP should also be identified accurately by setting $f_{\max} = 4$ GHz.

In practice, the procedure in Sec. II only calls for one loaded case, in order to access R_s and improve the ISEP accuracy. Tests showed that the accuracy is fundamentally load-independent if $\tau_{a,2}/\tau_{a,1}$>10, even though no hard threshold appeared, as discussed below. Case 9 was chosen for the second ACF dataset required by Phase 2, since it ensures $\tau_{a,2}/\tau_{a,1} \simeq 20$. In order to further stress the robustness of this method, only 25 frequency samples were used, out of 50 used for the results in Tab. I. Fig. 4 compares the ACF R predicted for the two- and six-element stirrers for k={1, 3}, by only using data for case 1 (dashed lines) and then also adding results for case 9 (solid lines). The first phase accurately predicts the ACF across all eleven cases for the two-element stirrer, with phase 2, including case 9 data, only bringing marginal improvement. For the six-element stirrer with k=3 the situation is different, since the significantly smaller τ_s implies a lower cutoff frequency f_o (cf. Tab. I), thus with less opportunities to observe how R_s evolves over frequency. The CIs (shaded areas) in Fig. 4 show that the additional load-case data improves the prediction to the point of yielding results with smaller uncertainty than direct ACF measurements.

TABLE II: ACF PREDICTION ACCURACY (RMS ΔR)

$f_{\max}$	cases	No. of stirrer el. and rotation increment k								
		2 el.			4 el.			6 el.		
		k: 1	2	3	1	2	3	1	2	3
8 GHz	1	0.02	0.04	0.03	0.02	0.03	0.07	0.02	0.04	0.07
	1+5	0.02	0.04	0.05	0.02	0.05	0.05	0.02	0.04	0.06
	1+7	0.02	0.03	0.04	0.02	0.04	0.04	0.02	0.04	0.04
	1+9	0.02	0.03	0.03	0.02	0.03	0.03	0.02	0.04	0.04
4 GHz	1	0.02	0.04	0.03	0.02	0.03	0.07	0.02	0.04	0.07
	1+5	0.02	0.04	0.04	0.04	0.06	0.06	0.02	0.05	0.06
	1+7	0.02	0.04	0.05	0.03	0.05	0.05	0.02	0.03	0.04
	1+9	0.02	0.04	0.04	0.02	0.03	0.04	0.02	0.03	0.04

The impact of insufficient loading on the ISEP accuracy can be appreciated in Fig. 5, for $k = 3$. Case 9 is sufficient to yield results almost overlapping with the reference results found using all the 11 datasets, while with case 5 errors are between 20 and 30 % off. Setting $f_{\max} = 4$ GHz (12 freq. samples) has a similarly limited impact, while cutting it back to 2 GHz (6 samples) leads to a loss of accuracy, since now the condition $f_{\max} > f_o$ is no longer met. As already noted, for the six-element stirrer, relying only on case 1 is no longer sufficient, because of its small f_o, making R_s only accessible at low frequency, leading to an almost 100% error on the ISEP. This situation, observed for $k = 3$, is to be expected also for larger stirrers operated at $k = 1$: a stirrer with a surface ten times larger would feature the same τ_s, based on a_o in Tab. I.

Prediction errors for the ACF are shown in Tab. II, confirming that data from an unloaded RC ensure a consistently good accuracy for all cases tested, apart for k=3. Including data from a loaded RC provides more stable and accurate predictions, as long as losses are large enough to ensure access to R_s, with case 5 indeed presenting larger errors. Tests limited to just 12 frequencies up to 4 GHz also provide accurate ACF prediction up to 8 GHz, confirming the ability of the proposed procedure to extrapolate the stirrer efficiency under a wide range of conditions, avoiding preliminary measurements for each new test configuration.

V. CONCLUSIONS

This letter has introduced a new methodology to predict from frequency-domain data how varying loading conditions in an RC affect its ability to generate independent testing scenarios. It does neither require complex data processing, nor large datasets over wide bands. As little as 12 frequency samples spread over 4 GHz were shown to provide accurate predictions for eleven loading conditions tested up to 8 GHz. It is possible to rely just on data acquired in an unloaded RC, but the addition of results from a loaded RC ensures more robust predictions with uniform accuracy. Future work will extend this technique to the case of multiple stirrers.

REFERENCES

[1] P. Kildal, "Overview of 6 years R&D on characterizing wireless devices in Rayleigh fading using reverberation chambers," in *Intern. Workshop on Antenna Technology (IWAT), 2007*. IEEE, 2007, pp. 162–165.

[2] C. Holloway, D. Hill, J. Ladbury, P. Wilson, G. Koepke, and J. Coder, "On the use of reverberation chambers to simulate a rician radio environment for the testing of wireless devices," *IEEE Trans. Antennas Propag.*, vol. 54, no. 11, pp. 3167–3177, Nov 2006.

[3] M. A. Garcia-Fernandez, J. D. Sanchez-Heredia, A. M. Martinez-Gonzalez, D. A. Sanchez-Hernandez, and J. F. Valenzuela-Valdes, "Advances in mode-stirred reverberation chambers for wireless communication performance evaluation," *IEEE Communications Magazine*, vol. 49, no. 7, pp. 140–147, 2011.

[4] X. Chen, J. Tang, T. Li, S. Zhu, Y. Ren, Z. Zhang, and A. Zhang, "Reverberation chambers for over-the-air tests: An overview of two decades of research," *IEEE Access*, vol. 6, pp. 49 129–49 143, 2018.

[5] A. Sorrentino, G. Ferrara, and M. Migliaccio, "The reverberating chamber as a line-of-sight wireless channel emulator," *IEEE Trans. Antennas Propag.*, vol. 56, no. 6, pp. 1825–1830, 2008.

[6] C. Patané Lötbäck, A. Skårbratt, and C. Ornelius, "Extending the reverberation chamber using a channel emulator for characterisation of over-the-air performance of multiple-input-multiple-output wireless devices," *Science, Measurement Technology, IET*, vol. 9, no. 5, pp. 555–562, 2015.

[7] K. A. Remley, J. Dortmans, C. Weldon, R. D. Horansky, T. B. Meurs, C.-M. Wang, D. F. Williams, C. L. Holloway, and P. F. Wilson, "Configuring and verifying reverberation chambers for testing cellular wireless devices," *IEEE Trans. Electromagn. Compat.*, vol. 58, no. 3, pp. 661–672, 2016.

[8] F. Moglie and V. M. Primiani, "Analysis of the independent positions of reverberation chamber stirrers as a function of their operating conditions," *IEEE Trans. Electromagn. Compat.*, vol. 53, no. 2, pp. 288–295, 2011.

[9] R. J. Pirkl, K. A. Remley, and C. S. L. Patané, "Reverberation chamber measurement correlation," *IEEE Trans. Electromagn. Compat.*, vol. 54, no. 3, pp. 533–545, 2012.

[10] X. Chen, "Experimental investigation of the number of independent samples and the measurement uncertainty in a reverberation chamber," *IEEE Trans. Electromagn. Compat.*, vol. 55, no. 5, pp. 816–824, 2013.

[11] G. Esposito, G. Gradoni, F. Moglie, and V. M. Primiani, "Stirrer performance of reverberation chambers evaluated by time domain fidelity," in *2013 IEEE Inter. Symp. on Electromagn. Compat.* IEEE, 2013, pp. 207–212.

[12] M. G. Becker, M. Frey, S. Streett, K. A. Remley, R. D. Horansky, and D. Senic, "Correlation-based uncertainty in loaded reverberation chambers," *IEEE Trans. Antennas Propag.*, vol. 66, no. 10, pp. 5453–5463, 2018.

[13] CTIA, "Test plan for wireless large-form-factor device over-the-air performance," 2016.

[14] 3GPP, "Enhanced over-the-air test methods for NR FR1 total radiated power and total radiated sensitivity - release 18," 2023.

[15] J. N. Dortmans, K. A. Remley, D. Senić, C.-M. Wang, and C. L. Holloway, "Use of absorption cross section to predict coherence bandwidth and other characteristics of a reverberation chamber setup for wireless-system tests," *IEEE Trans. Electromagn. Compat.*, vol. 58, no. 5, pp. 1653–1661, 2016.

[16] A. Cozza, "Stirring coherence time to predict stirrer efficiency in loaded reverberation chambers," *IEEE Trans. Electromagn. Compat.*, vol. 66, no. 1, pp. 37–48, 2024.

[17] ——, "A framework for comparing and predicting stirrer efficiencies in different reverberation chambers," *IEEE Trans. Electromagn. Compat.*, vol. 66, no. 3, pp. 684–693, 2024.

[18] K. A. Remley, R. J. Pirkl, H. A. Shah, and C.-M. Wang, "Uncertainty from choice of mode-stirring technique in reverberation-chamber measurements," *IEEE Trans. Electromagn. Compat.*, vol. 55, no. 6, pp. 1022–1030, 2013.

[19] N. Wellander, O. Lundén, and M. Bäckström, "Experimental investigation and mathematical modeling of design parameters for efficient stirrers in mode-stirred reverberation chambers," *IEEE Trans. Electromagn. Compat.*, vol. 49, no. 1, pp. 94 –103, feb. 2007.

[20] C. L. Lawson and R. J. Hanson, *Solving least squares problems*. Prentice-Hall Inc., Englewood Cliffs, New Jersey, USA, 1974.

[21] A. Bowley, "The standard deviation of the correlation coefficient," *Journal of the American Statistical Association*, vol. 23, no. 161, pp. 31–34, 1928.

[22] W. H. Press, W. T. Vetterling, S. A. Teukolsky, and B. P. Flannery, *Numerical recipes, 3rd edition: The art of scientific computing*. Cambridge University Press, Cambridge, UK, 2007.

[23] C. Lemoine, P. Besnier, and M. Drissi, "Estimating the effective sample size to select independent measurements in a reverberation chamber," *IEEE Trans. Electromagn. Compat.*, vol. 50, no. 2, pp. 227–236, May 2008.

[24] E. Genender, C. Holloway, K. Remley, J. Ladbury, G. Koepke, and H. Garbe, "Simulating the multipath channel with a reverberation chamber: Application to bit error rate measurements," *IEEE Trans. Electromagn. Compat.*, vol. 52, no. 4, pp. 766–777, Nov 2010.

[25] P.-S. Kildal, X. Chen, C. Orlenius, M. Franzén, and C. S. L. Patané, "Characterization of reverberation chambers for OTA measurements of wireless devices: Physical formulations of channel matrix and new uncertainty formula," *IEEE Trans. Electromagn. Compat.*, vol. 60, no. 8, pp. 3875–3891, 2012.

[26] C. L. Holloway, H. A. Shah, R. J. Pirkl, W. F. Young, D. A. Hill, and J. Ladbury, "Reverberation chamber techniques for determining the radiation and total efficiency of antennas," *IEEE Trans. Antennas Propag.*, vol. 60, no. 4, pp. 1758–1770, April 2012.

[27] D. A. Hill, *Electromagnetic fields in cavities: deterministic and statistical theories*. John Wiley & Sons, 2009.